The Effect Of An Equatorial Continent On The Tropical Rain Belt. Part 2: Summer Monsoons

Michela Biasutti* Spencer Hill,

Lamont-Doherty Earth Observatory of Columbia University, 61 Route 9W, Palisades, NY 10964.

Aiko Voigt

Department of Meteorology and Geophysics, University of Vienna, Austria.

**Corresponding author address:* Lamont-Doherty Earth Observatory of Columbia University, 61 Route 9W, Palisades, NY 10964.

E-mail: biasutti@ldeo.columbia.edu

ABSTRACT

The Tropical Rain belts with an Annual cycle and Continent Model Intercomparison Project (TRACMIP) ensemble includes slab-ocean aquaplanet control simulations and experiments with a highly idealized tropical continent. We compare the two set-ups to investigate monsoon development and contrast the characteristics of oceanic and continental rain bands in GCMs with CMIP5-class dynamics and physics. Over land, the rainy season occurs close to the time of maximum insolation. Other than in its timing, the continental rain band remains in an ITCZ-like regime, consistent with expectations for deep-tropical monsoons: a smooth latitudinal transition, a poleward reach only slightly farther than the oceanic ITCZ's, and a constant width throughout the year. This monsoon confinement to the deep tropics is the result of a tight coupling between regional rainfall and circulation anomalies: ventilation of the lower troposphere by the anomalous meridional circulation is the main limiting mechanism, while ventilation by the mean westerlies is only secondary. Comparison of two sub-sets of TRACMIP simulations indicates that a low heat capacity determines, to a first degree, both the timing and the strength of the regional solsticial circulation; this lends support to the choice of idealizing land as a thin slab ocean in much theoretical literature on monsoon dynamics. Yet, both the timing and strength of the monsoon are strongly modulated by the treatment of evaporation over land and by the interaction of moisture and radiation. This points to the need for a fuller exploration of land characteristics in the hierarchical modeling of the tropical rain bands.

1. Introduction

The last twenty years have seen much progress towards a theory of monsoon circulations (Geen et al. 2020). It has become apparent that individual regional monsoons should not be regarded as the product of local land-sea contrast (Gadgil 2003), but rather elements of a coherent global monsoon (Wang and Ding 2008), integral parts of the planetary Hadley circulation and of the intertropical convergence zone (ITCZ). This recognition has lead to theories of monsoons that rely only on zonal mean dynamics (Bordoni and Schneider 2008; Schneider et al. 2014). Nevertheless, for the zonal circulation to achieve its solstitial, approximately angular-momentum-conserving regime the surface boundary must have low heat capacity (Geen et al. 2019). On Earth, this means: that continents are necessary; that the oceanic ITCZ would not behave as the observed zonal mean rain band behaves; and that, instead, the regional monsoons shape the seasonality of the zonal mean circulation. These considerations imply that Earth's zonal asymmetries and localized monsoons are essential to the zonal mean circulation (Dima et al. 2005; Shaw et al. 2015). Recently, Geen et al. (2019) have argued that there exist two classes of monsoon circulations, one that behaves more like a canonical ITCZ, with smooth seasonal transitions and weaker overturning circulation, and one that is characterized by abrupt onset and an angular-momentum conserving cross-equatorial cell. In the first class are those monsoons that are confined to about 10 degrees of the equator (such as the West African and the Australian monsoon), in the second class are those monsoons that are centered at more subtropical locations (e.g., the Indian monsoon). But what determines the location of monsoon rainfall? We still lack a theory of the tropical rain bands that is complete enough to predict this from first principles (Biasutti et al. 2018; Hill 2019).

The Tropical Rain belts with and Annual cycle and Continent Model Inter-comparison Project (Voigt et al. 2016, TRACMIP,) was implemented to addresses the relationship between monsoons

and the ITCZ in a set of climate models with CMIP5-class dynamics and physical parameterizations. The experimental design *assumes* that the presence of a tropical continent will generate a monsoon: the control set up is a slab-ocean aquaplanet while the monsoon set up includes an idealized rectangular continent straddling the equator. In a companion paper (Biasutti et al. 2021) we focused on how the regional monsoon circulation affected the annual mean state of the ITCZ. In this paper, we focus on the monsoon circulation itself. Our first task is comparing the simulated continental and oceanic rain bands to each other and to measures of the monsoon and ITCZ "regimes". Does the continental rain band in TRACMIP show an enhanced poleward movement (Geen et al. 2019) or extent (Gadgil 2003)? Does it transition between the dry and rainy seasons with the rapidity of a monsoon (Bordoni and Schneider 2008) or the smoothness of an ITCZ (Geen et al. 2019)? How sensitive is the spatial extent of the monsoon to commonly used definitions based on wind (Ramage 1971), or rainfall (Webster et al. 1998; Wang and Ding 2008)?

As we will show (for example in Figure 1a,b), the TRACMIP monsoon remains confined to the deep tropics and evolves in an "ITCZ-like" regime similar to that of the West African monsoon (Geen et al. 2020). The limited reach of the monsoon in today's Africa is ascribed primarily to the presence of the desert to the north, which both reduces the energy input absorbed by the atmospheric column (Charney 1975; Chou and Neelin 2003) and is the source of low moist static energy (MSE) advected by the regional circulation (Hill et al. 2017). The TRACMIP set up, though, does not include deserts, and thus these mechanisms should not be relevant.

More generally, it has been argued that the poleward reach of the tropical rainfall is limited by influxes of low MSE. We refer to this process as "ventilation", expanding on the original meaning of the term in Chou et al. (2001). For both oceanic and continental rain, this influx can come from the midlatitudes (e.g., Chiang and Bitz 2005; Kang et al. 2008; Peterson and Boos 2020); conversely, the subtropical reach of the Indian monsoon is due to shielding of mid-latitude air by

the mountains (e.g., Boos and Kuang 2010). For the regional monsoons, low MSE can come from dry deserts (Hill et al. 2017) or cool oceans (Chou et al. 2001). Idealized studies on the spatial distribution of monsoon rainfall have concluded that land geometry is the key parameter, and that ventilation is the process that stops the monsoon from expanding poleward (Chou et al. 2001; Maroon and Frierson 2016; Zhou and Xie 2018).

Chou et al. (2001), using a continental geometry similar to TRACMIP's, ascribed the limited monsoon extent to the transport into the eastern domain of cool, marine air by a combination of the mean westerlies and an interactive "Rodwell-Hoskins" Rossby wave emanating from the monsoon rainfall itself. Their atmospheric model (QTCM, Neelin and Zeng 2000) only allowed for the barotropic and the first baroclinic mode of circulation, so both the mean westerlies and the anomalous circulation were features of the free troposphere. Zhou and Xie (2018), using a model with simplified physics but fully resolved vertical structure, also explained the ventilation of a simplified zonally confined continent in terms of the free tropospheric westerlies. Specifically, they claimed that westerlies bring colder temperature from the ocean over the continent and, as convection homogenizes the cooling down to the surface, they end up stabilizing the atmosphere and reducing rainfall. But conclusions from these earlier studies might depend on their severe idealizations of the atmosphere and, indeed, they seem at odds with our previous results in Biasutti et al. (2021): in TRACMIP, land influences the ocean downstream via boundary-layer winds, the anomalous circulation is important, and so are moist radiative feedbacks. Therefore, we make the examination of these processes' role in the ventilation of the monsoon a second focus of this study.

While the atmosphere in the TRACMIP models is simulated with full physics and full dynamics, the land surface is extremely idealized: the "continent" consists of modified slab-ocean aquaplanet grid cells with increased evaporative resistance, increased albedo, reduced heat capacity, and no ocean heat transport (as specified by q-fluxes). TRACMIP was not purposefully designed to ex-

plore the role of different idealizations, but fortuitous errors of implementation allow us to gain insight on the effects of each land characteristics. We have shown in Biasutti et al. (2021) that changes in heat capacity play a predominant role in the creation of solstitial anomalies over land and even of the annual mean anomalies over the ocean. Here, we again compare simulations where the continent has either reduced or unchanged heat capacity to show how the latter affects the continental rain band, in comparison to other land characteristics.

This paper is organized as follows. In Section 2 we describe in more details the model simulations and our analysis procedures. The following three sections contain the bulk of our results. First (Section 3), we provide an overview of the seasonal changes in the LandControl simulations and characterize the behavior of the oceanic and continental rain bands in terms of a set of descriptive measures of the monsoon and ITCZ "regimes". Second (Section 4), we provide more detail on the spatial pattern and poleward reach of the precipitation anomalies over the summer continent and we investigate whether ventilation is achieved by free-tropospheric or boundary-layer winds and by the mean or the anomalous circulation. And third (Section 5), we clarify the importance of a reduced heat capacity in driving the continental anomalies. Section 6 summarizes our results, discusses them in connection to previous idealized modeling of the monsoon, and provides our outlook for future research.

2. Data and methods

a. The TRACMIP protocol

Table 1 provides a list of TRACMIP models (Voigt et al. 2016) included in this study. All of the models include clouds and water vapor-radiation interactions, except the CaltechGray model, which assumes a fixed emissivity in the atmosphere and contains no clouds (Bordoni and Schnei-

der 2008). We compare AquaControl and LandControl simulations. AquaControl is an aquaplanet configuration with a slab ocean of 30m depth, zero eccentricity, atmospheric CO_2 concentrations of 348 ppmv, and a prescribed ocean heat transport convergence that is an idealized version of the observed zonal mean and that is the only source of asymmetry in the simulations under consideration. Because of this ocean heat flux, the NH is warmer than the SH in the annual mean. LandControl includes an idealized continent 45 degrees wide in longitude and extending in latitude from 30°N to 30°S. The idealization of land properties is accomplished by modifying ocean grid cells in the following ways: (1) the q-fluxes representing ocean heat transport convergence are zeroed out in the continent region (note that a uniform compensation over the ocean ensures zero net energy flux anomaly in the global mean); (2) the surface albedo over the continent is increased by 0.07; (3) the evaporation rate coefficient in the bulk moisture flux equation is halved; and (4) the heat capacity is reduced by changing the mixed layer depth from 30 m to 0.1 m.

We focus on the models that followed protocol exactly (hereafter, the protocol models; see the correction to Voigt et al. (2016) and discussion in Biasutti et al. (2021)), but we also briefly present results from models that incorporated the first three properties of land, but did not reduce the heat capacity of the continental region (hereafter, the MetUM models). We compare the MetUM to the protocol models in order to isolate the anomalies due to the choice of mixed layer depth from those due to other land characteristics. To ensure that our interpretation is correct, and that model choice is not an issue, we ensure that the inter-model scatter across the protocol models is much smaller than the difference between the protocol models and the MetUM models.

b. Rain Bands Diagnostics

We refer to zonal-mean quantities as "rain bands", with the understanding that the zonal average is calculated from global data in the AquaControl simulations and over just the continent (0-45W)

in the LandControl simulations. Land and ocean climatologies differ substantially in how fast either one responds to the external forcing coming from seasonally varying insolation. Therefore, LandControl–AquaControl differences emphasize the changes in the timing of the rainy season at any given latitude. If, instead, we compare the rain bands in their respective rainy seasons, we emphasize differences in structure and behavior, independent of timing.

We characterize the spatial extent, the position, the rapidity of onset and the characteristics of ascent (vertical profiles, frequency, and intensity) in the rain bands according to the quantities summarized below:

Monsoon Rainfall Following Wang and Ding (2008), we define monsoon regimes where (a) the local summer-minus-winter precipitation rate exceeds 2 mm day^{-1} and (b) the local summer precipitation exceeds 55% of the annual total. The first criterion distinguishes the monsoon climate from more arid climate regimes. The second ensures that precipitation is concentrated during local summer, thereby distinguishing the monsoon climate from equatorial perennial rainfall regimes. We define summer differently in the case of LandControl and AquaControl. For LandControl we take local summer to denote May through September for the NH and November through March for the SH. AquaControl seasons are shifted by three months (NH summer goes from August to December and SH summer from February through June).

Wind Reversal We identify regions of wind reversal as those regions where the maximum difference in wind direction for any pair of months is larger than 90 degrees, for non-negligible wind speed (the exact value of the threshold is unimportant) .

Rainband Position We calculate the position of the rain band as the centroid of precipitation following the definitions of Adam et al. (2016) and Voigt et al. (2014)[1], or as the latitude of maximum rainfall.

Rainband Migration Speed We take the time derivative of the 5-day running-mean smoothed daily values of the rain band position to calculate the meridional translation speed of the rain bands (Geen et al. 2019)

Rain Band Width Following Byrne and Schneider (2016), we define the width of the rain bands as the meridional distance where net precipitation (precipitation - evaporation, P-E) is positive.

Rain Characteristics We diagnose changes in rainfall characteristics in terms of frequency of rainy days (rain accumulation larger than 1mm day^{-1}) and simple daily rain intensity (rain intensity on rainy days in mm day^{-1}).

We use climatologies based on the last 20 years of monthly data or, when daily data are necessary, on 10 years of simulations.

3. Monsoon and ITCZ regimes: Diagnostics of Oceanic and Continental Rain Bands

Figure 1 shows the month-latitude Hoevmoeller diagrams of climatological fields that have been zonally averaged over the oceanic and continental sectors in the LandControl simulations; contours of the AquaControl climatology (zonally averaged) are superimposed on the LandControl sector averages in order to help the comparison. Besides the rain bands (Figure 1a,b), we show the seasonal evolution of surface temperature (Figure 1c,d), and low-level MSE (Figure 1e,f). The climatology of the LandControl simulation averaged over the ocean sector (left panels, Figure 1a,c,e)

[1]The Adam et al. (2016) definition is more weighted toward rainfall away from the equator and indicates a smaller seasonal excursion than the Voigt et al. (2014) definition, which calculates the latitude where there is as much tropical rainfall to the north as to the south.

is similar to the zonal mean of AquaControl, with only small differences in the timing and intensity of peak anomalies in all fields. This similarity is consistent with our findings in Biasutti et al. (2021), in which we show that the influence of land extends only about 120° to the west of the continent, leaving most of the ocean unaffected. In what follows, we select to contrast directly the oceanic rain band in the AquaControl and the continental rain band in the LandControl.

The most obvious difference between LandControl and AquaControl, and the expected result of a reduced surface heat capacity, is that the annual cycle is phase-shifted early over land, compared to the ocean, by between 1 and 2 months in all variables (right panels, Figure 1b,d,f). Peak values are also affected by land characteristics, but differently for different fields. Precipitation shows a small reduction in peak values, especially in the Northern Hemisphere. The surface temperature summer-to-winter seasonal excursions are of larger magnitude in LandControl than in AquaControl (as is also expected for a lower heat capacity system forced by oscillating heat fluxes). In contrast, seasonal MSE excursions remain similar across ocean and land, but MSE is overall reduced in LandControl. A lesser MSE maximum derives from the imposed reduction in local evaporation and also from transport of low MSE into the continent (see also Sec. 4).

The impression one derives from Figure 1 is that the oceanic and continental rain bands are overall very similar – aside from their phasing within the calendar year. Following Geen et al. (2019), we suggest that the TRACMIP monsoon is in a deep-tropical, ITCZ-like regime, namely a regime in which the monsoon never jumps to subtropical latitudes and never develops an approximately angular momentum conserving circulation. Yet, the behavior of the land-based rain band remains distinct from that of the oceanic ITCZ.

More detailed analysis supports this suggestion. Figure 2 shows the seasonal migration of the rain band (indicated by three definitions in different shades of blue), alongside the location of maximum surface temperature (red), maximum boundary layer MSE (magenta), and minimum

sea level pressure (black). In AquaControl, the maxima of surface temperature and MSE linger at their northernmost and southernmost positions and transition between the two rather quickly, more like square waves than sinusoids. The evolution of the oceanic rain band is more gradual, but also more asymmetric: the shift from South to North is quicker than the reverse. Over ocean, the relationship between the rain band and the position of the maximum MSE thus varies over the course of the seasonal march.

We have already noted that the evolution of the continental climate is shifted early. We now see that, in the NH, the timing of extrema in surface temperature, MSE, and SLP shifts more (from October to August) than that of the rain band (from October to September). In the SH, both the rain band and the surface extrema shift by the same amount, two months. Thus, the northward migration and the southward migration are now of the same duration. Moreover, while the loci of extreme temperature, MSE, and SLP are experiencing larger meridional excursion over land than over ocean, the rain band is not: it oscillates between 5°S and 10°N over both land and ocean. This causes a larger separation between the rain band and surface extrema (temperature, MSE, SLP) over land, compared to the ocean. The larger separation between the rain band and the minimum SLP (the Inter-Tropical Front, ITF) is a feature of real world monsoons, most famously in West Africa (Nicholson 2018) [2]. The separation of the rain band from the maximum in MSE is expected from theories of the zonally symmetric moist circulation, especially for off-equatorial ITCZs (e.g., Privé and Plumb 2007). Nevertheless, it is unclear why the magnitude of this displacement would be larger over land, given that the location of the rain band is similar in the two domains.

The relationships between the positions of the oceanic and continental maxima in low-level MSE and the corresponding rain bands is further explored in Figure 3, which shows one quantity

[2] Although the LandControl does not develop a dry shallow circulation reaching to the ITF, as the one seen in West Africa or Australia (Nie et al. 2010)

plotted against the other. The relationship is not one-to-one throughout the year. In the case of the oceanic ITCZ, the mismatch happens during the transition seasons, when the equatorial ITCZ is diffused and can correspond to an MSE maximum on either side of the equator. But in the case of the land monsoon, the mismatch (with similar ITCZ positions corresponding to a broad range of MSE maximum positions) is especially evident during the early summer, as rainfall progresses towards the poles, but does so slower than the MSE maximum. This behavior is opposite to the abrupt onset of aquaplanet monsoons (Bordoni and Schneider 2008), that occurs provided the mixed layer depth is sufficiently small (Wei and Bordoni 2018).

The degree of similarity in the progressions of the oceanic and continental rain bands is detailed in Figure 4. The top panels reveal that both rain bands reach similar northernmost and southernmost positions: there is less difference between the LandControl and AquaControl cases than across models of the ensemble or across two commonly used centroid definitions. The translation speeds (shown in Figure 4c,d for one centroid definition, but robust to the choice) are also somewhat similar between ocean and land, but with some noteworthy differences. Compared to the aquaplanet, migration speeds over the continent are generally faster and less consistent with a perfect sinusoidal progression (shown as an ellipse calculated from the annual harmonic). The onset of the land monsoon (first and third quadrants) is somewhat slower than its demise (second and fourth quadrants) in opposition to the behavior of the AquaControl ITCZ and to that reported for aquaplanet monsoons in Geen et al. (2019).

Figure 5 shows the evolution of the rain band width, as defined in Section 2. The two leftmost panels show latitude-month diagrams, while the right panel shows both the summer reach of the rain band in each hemisphere (vertical bars, left axis) and the maximum width of the rain band over the course of the year (markers, right axis). By either of these measures, the land-based rain band behaves in ways qualitatively similar to the ocean-based ITCZ, with the only difference that

it reaches slightly further poleward (especially in the SH) and is slightly wider throughout the year (but not in all models).

Finally, we move past the two-dimensional view of the monsoon in Figure 6, which shows the extent of the "global monsoon" as defined by the seasonality of rainfall and wind. The two definitions select for different regions: The rain-based monsoon region is nearly completely confined to the continent, extends to the subtropics, and is more extensive in the SH (where rainfall is concentrated in a shorter rainy season). The wind-based monsoon is elongated over the ocean, meridionally confined to the deep tropics, and is more extensive in the NH (where the circulation is stronger). Nevertheless, when we take the sector or zonal averages, both definitions are consistent in selecting for a slightly broader meridional span of the LandControl rain band, compared to the AquaControl.

In summary, the above analysis shows that the TRACMIP monsoons is a deep-tropical monsoon in an ITCZ-like regime, not too dissimilar from the West African monsoon. First, the width of the TRACMIP rain band is similar over land and ocean and close to constant throughout the year. Second, the rain's northernmost reach is similar in the two domains. Third, areas of positive P-E progress smoothly from one hemisphere to the other. Again, this behavior agrees with observations in the African sector: the maximum in rainfall jumps from the coastal ocean to the interior at the beginning of summer (Sultan and Janicot 2003), but the zonally averaged rainfall band progresses quite smoothly. Moreover, the transition over Africa is faster in its retreat than in its advance (Biasutti 2019), consistent with the behavior seen in the TRACMIP LandControl.

4. The poleward extent of the summer monsoon: Mechanisms of ventilation.

A map view of the LandControl-AquaControl seasonal anomalies provides clues to the processes that determine the extent of the TRACMIP monsoon. Figure 7 shows the surface temperature

(shaded) and precipitation (contour) anomalies for the four standard seasons; the AquaControl rain band is also shown for reference. Throughout the year, temperature and rainfall anomalies over land are consistent–in sign and strength–with the accelerated response of the continent to insolation (compared to the ocean) and with the tendency for rainfall to follow the net energy input into the atmosphere. This translates to small anomalies during equinox seasons (comparable to the annual mean anomalies, Biasutti et al. 2021) and much larger anomalies during the solstice seasons. Anomalies in both temperature and rainfall are positive in the summer hemisphere and negative in the winter hemisphere.

The wintertime cold anomalies are the largest, due to the reinforcing effects of enhanced resistance to evaporation and reduced energy input, further amplified by moist-radiative feedbacks and by the divergent surface circulation (Biasutti et al. 2021). Summertime and wintertime anomalies in rainfall are more comparable in their peak positive and negative values, but they differ greatly in shape. The wintertime dry anomalies are centered at the latitude of the AquaControl ITCZ and are roughly zonally oriented (both foregone consequences, to some degree, of no negative rainfall). The summertime wet anomalies extend poleward from the latitude of the AquaControl ITCZ and are characterized by a triangular pattern: they are narrow in the western part of the continent and broad in the eastern part, where they reach the coastlines at 30° N and S. A similar pattern of summertime rainfall anomalies has been interpreted (Chou et al. 2001; Zhou and Xie 2018) as the effect of ventilation, primarily by the mean free tropospheric westerlies. We find that ventilation happens by different mechanisms in TRACMIP.

Figure 8 shows fields relevant to ventilation in the two summer hemispheres: JJA above the equator and DJF below the equator. The top and bottom panels describe processes in the free troposphere and in the boundary layer, respectively. Figure 8a shows temperature anomalies at 300hPa (shaded), geopotential anomalies at 700hPa (contours) and the full LandControl wind at

700hPa (vectors). The mean westerlies are weak over the subtropical portion of the continent and the temperature anomalies do not resemble what we would expect from westerly advection: instead of decaying inland, they are strongest in the western part of the continent and they are warm in the summer hemisphere subtropics, opposite what is necessary for ventilation (Zhou and Xie 2018). Upper level temperatures are cold everywhere else and show the Gill-like signature (Gill 1980) of the negative rainfall anomalies in the oceanic cold tongue. It is possible that these cold temperatures are homogenized downward by convection and modulate rainfall and surface temperature in the core monsoon region. Nevertheless, they do not appear to be preventing rainfall in the western portion of the subtropical continent.

Figure 8b shows fields relevant to low-level processes (anomalies in precipitable water, boundary layer geopotential and wind) and suggests a predominant role for such processes in limiting the monsoon in the western portion of the continent and enhancing it in the East. Note, for example, the correspondence between the slanted positive anomalies in precipitable water over the summer continent and the low-level cyclonic circulation that brings tropical moist air to the eastern continent and subtropical dry air to the western continent.

The above suggestions are confirmed by a quantitative analysis of MSE advection. Figure 9a,b show the total MSE advection in the boundary layer and the free troposphere (925hPa and 300hPa, respectively; these levels were chosen as the most clearly representative, but results are robust to the choice) in the two summer hemispheres (JJA in the NH and DJF in the SH). The pattern of anomalies is similar at both levels, but the magnitude of the anomalies is much larger in the boundary layer. We decompose the advection in its zonal and meridional terms and further decompose those as the linear combination of the advection of anomalous MSE by the mean wind and advection of mean MSE by the anomalous wind. We obtain 4 terms that are plotted in Figure 9c through j. This decomposition highlights how MSE advection is achieved differently at different

levels. In the free troposphere, the mean westerlies acting on the anomalous gradient of MSE do indeed ventilate the western part of the continent, as suggested in the literature. But this effect is counteracted by the other terms, especially by the advection of the climatological MSE gradient by the anomalous meridional wind. Within the boundary layer, the dominant mechanism of ventilation is the advection of the background MSE gradient by the meridional component of the anomalous circulation. The background zonal wind is most relevant at the coastlines, where it acts to counteract the main advection pattern. The other terms are small over the subtropical continent. (We note as an aside that the anomalous negative MSE advection that extends past the continent at about 10° N is the result of the covariant term.)

The vertical profiles of the MSE transport terms (Figure 10) confirm the description above and add some insight on the scatter across models. Higher in the troposphere, the advection into the western subtropical continent of low oceanic MSE by the mean zonal wind is compensated by the advection of the mean MSE by the anomalous meridional wind. Each term is uncertain across the ensemble, but the cancellation is not, so that the total uncertainty in the free-troposphere ventilation is low. Lower in the boundary layer, the continent is ventilated by the anomalous meridional wind acting on the background gradient in MSE between the tropics and the midlatitudes. This is the dominant term in the column MSE budget and imparts its uncertainty to the total advection term.

We conclude that, in TRACMIP, the diffusion of MSE anomalies by the free-troposphere westerlies is an active mechanism, but not the one primarily responsible for the ventilation of the subtropics. The poleward extent of the monsoon rains, in its mean and its uncertainty, is predominantly a consequence of anomalous poleward flow in the boundary layer acting on the prevailing MSE field that decreases toward the pole.

5. Land idealizations: The effect of a reduced heat capacity

From the simplest model of a uniform surface layer forced by a sinusoidal heat source, we expect that the small phase shift between insolation and surface temperature over land derives from the reduced heat capacity of continental grid points. Yet, we have seen in Figures 1 and 4 that neither MSE nor, especially, rainfall, covary perfectly with temperature, so that the question of the role of different land characteristics on rainfall remains somewhat open.

To identify whether land characteristics other than heat capacity contribute to the simulated LandControl-AquaControl seasonal changes, we contrast the mean anomalies across models that exactly followed the TRACMIP protocol to those across the two MetUM models, in which a reduced heat capacity for land grid points was not imposed. Figure 11a,b show the latitude-month Hoevmoeller diagrams of LandControl-AquaControl rainfall anomalies (alongside the AquaControl rain band, for reference). The top panel shows alternating dipoles in rainfall anomalies in the protocol models, with wet anomalies preceding, and dry anomalies trailing, the AquaControl rain band. The mean state and the anomalies are close to being in quadrature, suggesting a shift in the seasonality and consistent with a much smaller annual-mean signal (Biasutti et al. 2021). The bottom panel (in which land does not have a reduced heat capacity) shows peak anomalies of similar magnitude, although the pattern is different. When idealized land retains a high heat capacity, positive equatorial anomalies persist through the year and the subtropical dry anomalies are limited to local summer, when they act to reduce the local maximum. Thus, the timing of the rainy season remains unaffected.

We check the robustness of these results by examining the rainfall anomalies in the individual protocol models and MetUM models averaged within the northern (Figure 12a) and southern Figure 12b) continent. Only the protocol models show the alternating positive and negative anomalies,

while the MetUM models show only dry anomalies, especially intense in correspondence of the main rainy season. We note that the CAM5-Nor model (magenta line), is an outlier among the protocol models, somewhat closer to the behavior of the MetUM models: drying associated with land characteristics besides heat capacity (evaporative resistance, albedo, and lack of heat transport convergence) has a more prominent role in this model. Nevertheless we will consider the ensemble mean of all protocol models and interpret mean phase shifts as due to changes in heat capacity.

Rainfall reduction in the continental subtropics occurs by different mechanisms when it is due primarily to a smaller heat capacity or primarily to a resistance to evaporation. Figure 11b and e show the LandControl-AquaControl changes in the frequency of rainy days in the two sets of models (protocol and MetUM); Figure 11c and f show the changes in daily intensity. Peak changes in intensity are around 8 mm day^{-1}, either in positive or in negative values and in both sets of models. Peak changes in rain frequency are much larger in the case of the protocol models, and much larger for negative than for positive anomalies. This asymmetry is consistent with the more pronounced wintertime circulation changes driven by the heat capacity-induced land-sea contrast (Figure 7, see also Biasutti et al. (2021) for a comparison with the MetUM models) and with a greater role for dynamics, as opposed to thermodynamics, in affecting the occurrence of rainy days rather than their intensity. In contrast, in the MetUM simulations, the imposed land characteristics do not create large circulation in and out of the continent and changes in rainfall are predominantly caused by thermodynamic properties and expressed as changes in intensity.

A reduced heat capacity also affects the profile of ascent in the rain band (Figure 13). Figures 13a,c show the latitude/pressure zonal and sector mean of vertical velocity for the SH summer (DJF in LandControl and MAM in AquaControl in the case of the protocol models, MAM in both LandControl and AquaControl in the case of the MetUM models). Figures 13b and d show each

model's profile in the ascent regions. For models with a reduced heat capacity over land, vertical ascent is larger in magnitude and much more top heavy over land than over ocean[3]. The omega profile remains unchanged in the case when land does not have a reduced heat capacity. This change in the vertical profile of ascent only depends on the different heat capacity of the lower boundary, not on where the rain band is in its seasonal march. It follows that the presence of a low heat capacity continent will influence the responsiveness of the rain band to MSE fluxes: deeper or shallower profiles of ascent are associated with larger or smaller moist stability (Raymond et al. 2009), thus modulating the relationship between the position of the rain band and MSE transport (see, e.g., Biasutti et al. 2018).

6. Conclusions

In this paper we have examined the rain band that develops over the idealized tropical continent in the LandControl simulations of the TRACMIP multi-model ensemble (Voigt et al. 2016). The continental rain band moves farthest poleward around summer solstice, 1-2 months preceding its oceanic counterpart. Whereas the rain band width, translation speed, and maximum rain rate differ modestly between land and ocean. Previous work (Geen et al. 2019) had suggested that subtropical monsoons abruptly develop an approximately angular-momentum conserving circulation, while those in which maximum rainfall remains within about 10° or 15° of the equator show a a weaker, smoothly changing circulation (dubbed an ITCZ-like regime). This distinction motivated our investigation of the mechanisms of ventilation that set the poleward reach of the TRACMIP monsoon. We find that the advection of low MSE into the subtropical land by the low-level anomalous meridional wind acting on the background distribution of moist static energy

[3]The NorESM model is an exception, but we have not adjusted the averaging period to match its continental summer; when that is done, it too has deeper ascent over land

is the predominant mechanism, while the advection of anomalous MSE by the mean westerlies is secondary. This means that what sets the anomalous circulation sets the position of the rainfall maximum. At the same time, the position of the rainfall maximum implies (Geen et al. 2019, according to) whether the circulation shifts to an approximately angular-momentum conserving regime. Together, these conditions signify a tight coupling between rainfall and circulation, more so in TRACMIP than in previous studies in which the effect of the background circulation was paramount.

These insights are helpful to assess idealized simulations of the tropical rain bands: what is retained and what is lost when we eliminate a process or an entire component of the climate system? To begin to answer this question—although within a linear framework that might be insufficient (Garfinkel et al. 2021)—we focus on how different idealizations play out in our results and in the theoretical literature on the the global monsoon and ITCZ.

(i) Vertical Wind Structure. The pivotal studies of Chou et al. (2001) and Chou and Neelin (2003) were carried out with QTCM-1, the first version of the Quasi-equilibrium Tropical Circulation Model (Neelin and Zeng 2000; Sobel and Neelin 2006). In its original formulation, QTCM simplified the vertical structure of the atmosphere to one with full-troposphere overturning cells and no boundary layer dynamics. By design, therefore, ventilation was the effect of bulk advection of mid-latitude oceanic low-MSE air by the column-integrated westerlies in both the basic state and the anomalous circulation (itself a product of the monsoonal rainfall, as in the work of Rodwell and Hoskins 1996). While the distribution of land rainfall in TRACMIP is not qualitatively different from that in QTCM, boundary-layer advection of low MSE by the anomalous meridional circulation is the key process. The advection by the free troposphere mean westerlies is an active process, but secondary, and mostly counteracted by meridional advection.

One caveat remains necessary: while the TRACMIP GCMs resolve the boundary layer, they do not reproduce a shallow circulation. Heat-low dynamics and transport by the dry return flow of the shallow circulation is, instead, though to be important for the behavior of the African or Australian monsoons (e.g., Shekhar and Boos 2017; Zhai and Boos 2017).

(ii) Continental Geometry. We have not investigated land geometry per se, but we have demonstrated a primary role for the low-level circulation in ventilating the monsoon, and we can speculate on how the continental geometry would matter, at least for tropical continents (subtropical continents have been recently investigated by Maroon and Frierson 2016; Zhou and Xie 2018; Hui and Bordoni 2021, among others). First of all, we can assume that a continent that extended to the surface westerlies would be responsive to those as well (just as the TRACMIP ocean responds to the advection by the mean easterlies, Biasutti et al. 2021). Second, because northerly MSE advection is key, a continent that extended into colder oceans, or that included a desert to its poleward flank, would experience greater ventilation.

It is more difficult to speculate on the effect of the width of the continent. Zhou and Xie (2018) suggested that the length scale of the oceanic influence over land is given by a balance between the time scales of upper-level advection and convective mixing. But their view presupposes that westerly cold advection is the predominant mechanism of ventilation. If boundary layer processes are instead predominant, the scale of the low-level continental low becomes key. How the latter depends on local and remote rainfall and cloud anomalies, as well as on the characteristics of the lower boundary, remains an open question.

(iii) Surface Evaporation. We suggest that the treatment of evaporation over land modulates the extent of the monsoon in several key ways. First, reduced evaporation contributes to the asymmetry between continental winter cooling and summer warming and to the drying of the equatorial

ocean (Biasutti et al. 2021). Therefore, we expect that the precise structure of the low-level circulation anomalies that ventilate the monsoon would depend on the choice of how water fluxes are parameterized at the land surface. Second, impaired evaporation makes continental rainfall more sensitive to ventilation (Chou et al. 2001). The similarity in the responses in TRACMIP (where an evaporative resistance crudely mimicked vegetation) and QTCM (where a bucket model mimicked soil moisture processes) suggests to us that, as long as evaporation is reduced over land, the means of such reduction are not a crucial choice. Third, we stress (again on the strength of previous literature, e.g. Chou et al. 2001) that a moist land, from which evaporation is always possible, prevents the development of the heat low and the important interaction of the deep tropical monsoon with the shallow circulation (Zhai and Boos 2017; Peyrille et al. 2016).

(iv) Moist Radiative Processes. Influential studies of the rain bands (ITCZ and monsoons, e.g., Bordoni and Schneider 2008; Bischoff and Schneider 2014; Zhou and Xie 2018, among many) have been carried out with a model (Frierson et al. 2007) that simplified atmospheric physics, and in particular did not include the radiative effects of water vapor and clouds. Reassuringly, the same model is shown here to behave consistently with the ensemble of protocol models. Nevertheless, the CALTECH model (with no moist-radiative feedbacks; Bordoni and Schneider 2008) and the NorESM model (with strong moist-radiative feedbacks; Biasutti et al. 2021) often stand out as outliers. This supports the conclusion of many previous studies (for example, Kang et al. 2009, Maroon and Frierson 2016, Byrne and Zanna 2020, Biasutti et al. 2021 and, for a comprehensive review, Voigt et al, 2021) that moist-radiative processes are of first order (quantitative, but not qualitative) importance for the dynamics of the tropical rain bands.

The above discussion points to the need to better formalize a modeling hierarchy for land. For other GCM components besides land, there is a recognized hierarchy of model complexity from

which researchers can choose the level best suited to their objectives. For example, the ocean can be represented with fixed (uniform or non-uniform) surface temperatures, a slab with specified q-fluxes, a column ocean, or a full dynamical ocean (Jeevanjee et al. 2017). It is not obvious what the equivalent hierarchy should look like for land models since there are so many potential properties to include and there might be different combinations with similar complexity. We agree that heat capacity is the most consequential of the land characteristics, the zeroth order influence on the timing and the strength of the solsticial circulations. Nevertheless, the TRACMIP experiments suggest that anything that affects surface evaporation is also a fundamental knob, capable of shaping the regional circulation and the type of monsoon regime that ensues. Interactive soil moisture (as in Chou et al. (2001)), or vegetation (as, most crudely, in TRACMIP) both fit the bill; so do albedo, which determines the energy available to evaporation, and surface roughness, which alters wind and thus evaporation. The ways in which these factors affect low-level MSE have not been investigated in the theoretical literature as thoroughly as for heat capacity and continental geometry, and they deserve a deeper exploration. We suggest the need for more sensitivity experiments with full-physics comprehensive GCM in which land's defining factors (surface roughness, albedo, soil moisture, and vegetation) can be explicitly tuned for their effect on evaporation. This will allow a land model hierarchy to come into greater focus, and we will be closer to the ideal where anyone who wants to study monsoon dynamics will have a clearly defined array of tools from which to select the one best suited to their research.

Acknowledgments. Michela Biasutti, Aiko Voigt and the overall TRACMIP project were supported by the National Science Foundation under award # AGS-1565522. AV received support from the German Ministry of Education and Research (BMBF) and FONA: Research for Sustain-

able Development (www.fona.de) under grant 01LK1509A. MB and SAH acknowledge support from the Monsoon Mission Project under Indias Ministry of Earth Sciences

We thank Charles Blackmon-Luca for his help with data and software and Rick Russotto for ongoing discussions and his contribution to a previous version of this paper. We especially thank the modeling groups responsible for the creation of TRACMIP and of CMIP6. The model data used in this study are available in Google cloud (https://console.cloud.google.com/storage/browser/cmip6), thanks to a grant to the Pangeo project (https://pangeo.io/). Further information on TRACMIP, including sample scripts on how to access its data via Pangeo, is provided at https://gitlab.phaidra.org/voigta80/tracmip.

References

Adam, O., T. Bischoff, and T. Schneider, 2016: Seasonal and interannual variations of the energy flux equator and ITCZ. Part I: Zonally averaged ITCZ position. *Journal of Climate*, **29 (9)**, 3219–3230.

Biasutti, M., 2019: Rainfall trends in the African Sahel: Characteristics, processes, and causes. *Wiley Interdisciplinary Reviews: Climate Change*, **10 (4)**, e591.

Biasutti, M., R. D. Russotto, A. Voigt, and C. C. Blackmon-Luca, 2021: The Effect of an Equatorial Continent on the Tropical Rain Belt. Part I: Annual Mean Changes in the ITCZ. *Journal of Climate*, **34 (14)**, 5813–5828.

Biasutti, M., and Coauthors, 2018: Global energetics and local physics as drivers of past, present and future monsoons. *Nature Geoscience*, **11 (6)**, 392–400.

Bischoff, T., and T. Schneider, 2014: Energetic Constraints on the Position of the Intertropical Convergence Zone. *Journal of Climate*, **27 (13)**, 4937–4951.

Boos, W. R., and Z. Kuang, 2010: Dominant control of the South Asian monsoon by orographic insulation versus plateau heating. *Nature*, **463 (7278)**, 218–222.

Bordoni, S., and T. Schneider, 2008: Monsoons as eddy-mediated regime transitions of the tropical overturning circulation. *Nature Geoscience*, **1 (8)**, 515–519.

Byrne, M. P., and T. Schneider, 2016: Narrowing of the ITCZ in a warming climate: Physical mechanisms. *Geophysical Research Letters*, **43 (21)**, 11,350–11,357.

Byrne, M. P., and L. Zanna, 2020: Radiative Effects of Clouds and Water Vapor on an Axisymmetric Monsoon. *Journal of Climate*, **33 (20)**, 8789–8811.

Charney, J. G., 1975: Dynamics of deserts and drought in the Sahel. *Quart. J. Roy. Meteor. Soc, 101, 193*, **101**, 193–202.

Chiang, J., and C. M. Bitz, 2005: Influence of high latitude ice cover on the marine Intertropical Convergence Zone. *Climate Dynamics*, **25 (5)**, 477–496.

Chou, C., J. Neelin, and H. Su, 2001: Ocean-atmosphere-land feedbacks in an idealized monsoon. *Q. J. R. Meteorol. Soc.*, **127**, 1869–1891.

Chou, C., and J. D. Neelin, 2003: Mechanisms Limiting the Northward Extent of the Northern Summer Monsoons over North America, Asia, and Africa*. *Journal of Climate*, **16 (3)**, 406–425.

Dima, I. M., J. M. Wallace, and I. Kraucunas, 2005: Tropical Zonal Momentum Balance in the NCEP Reanalyses. *Journal of the Atmospheric Sciences*, **62 (7)**, 2499–2513.

Frierson, D. M. W., J. Lu, and G. Chen, 2007: Width of the Hadley cell in simple and comprehensive general circulation models. *Geophysical Research Letters*, **34 (18)**, 224.

Gadgil, S., 2003: The Indian Monsoon and its Variability. *Annu. Rev. Earth Planet. Sci.*, **31 (1)**, 429–467.

Garfinkel, C. I., I. White, and E. P. Gerber, 2021: Nonlinear Interaction between the Drivers of the Monsoon and Summertime Stationary Waves. *Geophysical Research Letters*, **48 (14)**, e2020GL092 321.

Geen, R., S. Bordoni, D. Battisti, and K. L. Hui, 2020: Monsoons, ITCZs, and the Concept of the Global Monsoon . *Reviews of Geophysics*, **58 (4)**.

Geen, R., F. H. Lambert, and G. K. Vallis, 2019: Processes and Timescales in Onset and Withdrawal of "Aquaplanet Monsoons". *J. Atmos. Sci.*, **76 (8)**, 2357–2373.

Gill, A. E., 1980: Some simple solutions for heat-induced tropical circulation. *Quarterly Journal of the Royal Meteorological Society*, **106 (449)**, 447–462.

Hill, S. A., 2019: Theories for Past and Future Monsoon Rainfall Changes. *Current Climate Change Reports*, **5 (3)**, 1–12.

Hill, S. A., Y. Ming, I. M. Held, and M. Zhao, 2017: A Moist Static Energy Budget–Based Analysis of the Sahel Rainfall Response to Uniform Oceanic Warming. *Journal of Climate*, **30 (15)**, 5637–5660.

Hui, K. L., and S. Bordoni, 2021: Response of Monsoon Rainfall to Changes in the Latitude of the Equatorward Coastline of a Zonally Symmetric Continent. *J. Atmos. Sci.*, **78 (5)**, 1429–1444.

Jeevanjee, N., P. Hassanzadeh, S. Hill, and A. Sheshadri, 2017: A perspective on climate model hierarchies. *Journal of Advances in Modeling Earth Systems*, **9 (4)**, 1760–1771, doi:10.1002/2017MS001038.

Kang, S. M., D. M. W. Frierson, and I. M. Held, 2009: The Tropical Response to Extratropical Thermal Forcing in an Idealized GCM: The Importance of Radiative Feedbacks and Convective Parameterization. *Journal of the Atmospheric Sciences*, **66 (9)**, 2812–2827.

Kang, S. M., I. M. Held, D. M. W. Frierson, and M. Zhao, 2008: The Response of the ITCZ to Extratropical Thermal Forcing: Idealized Slab-Ocean Experiments with a GCM. *Journal of Climate*, **21 (14)**, 3521–3532.

Maroon, E. A., and D. M. W. Frierson, 2016: The impact of a continent's longitudinal extent on tropical precipitation. *Geophysical Research Letters*, **43 (22)**, 11,921–11,929.

Maroon, E. A., D. M. W. Frierson, S. M. Kang, and J. Scheff, 2016: The Precipitation Response to an Idealized Subtropical Continent. *Journal of Climate*, **29 (12)**, 4543–4564.

Neelin, J., and N. Zeng, 2000: A quasi-equilibrium tropical circulation model—Formulation. *J. Atmos. Sci.*, **57**, 1741–1766.

Nicholson, S. E., 2018: The ITCZ and the Seasonal Cycle over Equatorial Africa. *Bulletin of the American Meteorological Society*, **99 (2)**, 337–348.

Nie, J., W. R. Boos, and Z. Kuang, 2010: Observational Evaluation of a Convective Quasi-Equilibrium View of Monsoons. *Journal of Climate*, **23 (16)**, 4416–4428.

Peterson, H. G., and W. R. Boos, 2020: Feedbacks and eddy diffusivity in an energy balance model of tropical rainfall shifts. *npj Climate and Atmospheric Sciences*, **3 (11)**.

Peyrille, P., J. P. Lafore, and A. Boone, 2016: The annual cycle of the West African monsoon in a two-dimensional model: mechanisms of the rain-band migration. *Quarterly Journal of the Royal Meteorological Society*, **142 (696)**, 1473–1489.

596 Privé, N. C., and R. A. Plumb, 2007: Monsoon dynamics with interactive forcing. Part I: Axisym-
597 metric studies. *Journal of the Atmospheric Sciences*, **64 (5)**, 1417–1430, doi:10.1175/JAS3916.
598 1.

599 Ramage, C. S., 1971: *Monsoon Meteorology*. Atmosphere, Ocean and Climate Dynamics, Aca-
600 demic Press, New York and London.

601 Raymond, D., S. Sessions, A. H. Sobel, and Z. Fuchs, 2009: The mechanics of gross moist stabil-
602 ity. *J. Adv. Model. Earth Syst*, **1 (9)**, 1–20.

603 Rodwell, M. J., and B. J. Hoskins, 1996: Monsoons and the dynamics of deserts. *Q. J. R. Meteorol.*
604 *Soc.*, **122**, 1385–1404.

605 Schneider, T., T. Bischoff, and G. H. Haug, 2014: Migrations and dynamics of the intertropical
606 convergence zone. *Nature*, **513 (7516)**, 45–53.

607 Shaw, T. A., A. Voigt, S. M. Kang, and J. Seo, 2015: Response of the intertropical convergence
608 zone to zonally asymmetric subtropical surface forcings. *Geophysical Research Letters*, **42 (22)**,
609 9961–9969.

610 Shekhar, R., and W. R. Boos, 2017: Weakening and Shifting of the Saharan Shallow Meridional
611 Circulation During Wet Years of the West African Monsoon . *Journal of Climate*.

612 Sobel, A. H., and J. Neelin, 2006: The boundary layer contribution to intertropical convergence
613 zones in the quasi-equilibrium tropical circulation model framework. *Theoretical and Compu-*
614 *tational Fluid Dynamics*, **20 (5)**, 323–350.

615 Sultan, B., and S. Janicot, 2003: The West African Monsoon Dynamics. Part II: The Preonset and
616 Onset of the Summer Monsoon. *Journal of Climate*, **16 (21)**, 3407–3427.

Voigt, A., N. Albern, P. Ceppi, K. Grise, Y. Li, and B. Medeiros, 2021: Clouds, radiation, and atmospheric circulation in the present-day climate and under climate change. *Wiley Interdisciplinary Reviews: Climate Change*, **12 (2)**, e694.

Voigt, A., S. Bony, J.-L. Dufresne, and B. Stevens, 2014: The radiative impact of clouds on the shift of the Intertropical Convergence Zone. *Geophysical Research Letters*, **41 (12)**, 4308–4315.

Voigt, A., and Coauthors, 2016: The tropical rain belts with an annual cycle and a continent model intercomparison project: TRACMIP. *J. Adv. Model. Earth Syst*, **8 (4)**, 1868–1891.

Wang, B., and Q. Ding, 2008: Global monsoon: Dominant mode of annual variation in the tropics. *Dynamics of Atmospheres and Oceans*, **44 (3-4)**, 165–183.

Webster, P., V. O. Magana, and T. N. Palmer, 1998: Monsoons: Processes, predictability, and the prospects for prediction. *Journal of Geophysical Research-Oceans*, **103 (C7)**, 14 451–14 510.

Wei, H. H., and S. Bordoni, 2018: Energetic Constraints on the ITCZ Position in Idealized Simulations With a Seasonal Cycle. *Journal of Advances in Modeling Earth Systems*, **10 (7)**, 1708–1725.

Zhai, J., and W. R. Boos, 2017: The drying tendency of shallow meridional circulations in monsoons. *Quarterly Journal of the Royal Meteorological Society*, **143 (708)**, 2655–2664.

Zhou, W., and S.-P. Xie, 2018: A Hierarchy of Idealized Monsoons in an Intermediate GCM. *Journal of Climate*, **31 (22)**, 9021–9036.

LIST OF TABLES

Atmospheric model	Component of	Protocol
CaltechGray	N/A	yes
CAM3	CCSM3	yes
CAM4	CCSM4	yes
CAM5Nor	NorESM2	yes
CNRM-AM5	CNRM-CM5	yes
ECHAM6.1	MPI-ESM	yes
MetUM-CTL*	GA6.0	no: heat capacity as in AquaControl
MetUM-ENT*	GA6.0 (modified)	no: heat capacity as in AquaControl
MIROC5 (atmospheric component)	MIROC5	yes
MPAS (atmospheric component)	MPAS	yes

TABLE 1. List of atmospheric GCMs used in this study, along with the coupled Earth System model that each atmospheric model is a component of, if applicable. Only the models following protocol (not starred) are included in the multi-model means. All models except CaltechGray are full physics GCMs. Citations and additional details such as model resolution are listed in Voigt et al. (2016).

LIST OF FIGURES

Fig. 7. Maps of the surface temperature (shaded) and precipitation (black contours, every 2mm day^{-1}, skipping the zero contour) LandControl minus AquaControl ensemble-mean seasonal anomalies. The seasonal means are DJF (a), MAM (b), JJA (c) and SON (d). The position of the AquaControl rain band for each season (as indicated by the 6mm day^{-1} contour) is superimposed in grey for reference. 41

Fig. 8. Top (a): summertime (JJA in the NH and DJF in the SH) ensemble mean LandControl minus AquaControl ensemble-mean anomalies in 300hPa temperature (shaded) and in 700hPa geopotential (contours, contour interval is 8m; dashed lines indicate negative anomalies, the zero contour is omitted), and 700hPa LandControl full wind field (vectors; only wind speeds greater than 3m/s are plotted; see reference arrow on the left). Summertime rainfall anomalies less than -2mm day^{-1} are shaded in brown and those greater than 2 (4) are shaded in green (dark green); Bottom (b): Same as in (a), but shading indicates 925hPa geopotential heights; contours indicate precipitable water (contour interval is 5g Kg^{-1}); and wind vectors are for the 925hPa anomalies (only wind speeds larger than 1m/s are plotted, see reference arrow on the left). 42

Fig. 9. Maps of summertime (JJA in the NH and DJF in the SH) LandControl minus AquaControl ensemble-mean anomalous MSE transport at 925hPa (left: a,c,e,g,i) and 300hPa (right: b,d,f,h,l). The total advection anomalies are given in the top panels (a,b). The other panels show: (c,d) the advection of the anomalous MSE gradient by the basic-state zonal wind; (e,f) the advection of the basic-state MSE gradient by the anomalous zonal wind; (g,h) the advection of the anomalous MSE gradient by the basic-state meridional wind; and (i,l) the advection of the basic-state MSE gradient by the anomalous meridional wind. Units are in $^{\circ}$C m s^{-1} (lat/lon degree)$^{-1}$. 44

Fig. 10. Vertical average profile of summertime (JJA in the NH and DJF in the SH) LandControl minus AquaControl ensemble-mean anomalous MSE transport in the western subtropical corners of the TRACMIP continent. The total advection anomalies are given in black (the sum of the linearized terms is given in the dashed black line). Blu refers to the advection by the mean wind of the anomalous MSE, magenta refers the advection by the anomalous wind of the mean MSE. Dotted lines refer to zonal terms and dash-dotted lines to meridional terms. The dominant terms are indicated in the legend and are plotted with a shading corresponding to plus or minus one standard deviation in the multi-model ensemble. The vertical axis is pressure in hPa; the MSE transport terms are calculated in units of $^{\circ}$C m s^{-1} (lat/lon degree)$^{-1}$. 45

Fig. 11. Latitude/time Hoevmoeller diagram of climatological LandControl minus AquaControl multi-model-mean monthly anomalies in (a,d) rainfall in mm day^{-1} (b,d) frequency of rainy days in percentage, and (c,f) simple daily intensity index in mm day^{-1}. Superimposed on the shaded fields are (a,d) the AquaControl climatological rainfall (gray contours) and (b,c,e,f) the LandControl-AquaControl monthly rainfall anomalies (contours colored according to the colorbar in a). Top (a,b,c) is for the mean of the models with reduced heat capacity over land. Bottom (d,e,f) is for the average of the models with unchanged heat capacity. 46

Fig. 12. The annual cycle of LandControl minus AquaControl rainfall anomalies averaged zonally (LandControl data over the continental sector only) and over (a) 10°15° N and (b) 10°15° S . The solid thin colored lines are individual models that followed protocol, the thick solid black line is their multi-model mean, and the light shading indicates a spread of $\pm$ 1 standard deviation. The dash-dotted lines are the two models that did not reduce heat capacity in the continental area. 47

738 **Fig. 13.** The effect of heat capacity on ascent profiles. (a) Vertical velocity omega profiles during SH
739 summer in LandControl (DJF, shaded, averaged over the continental sector) and AquaCon-
740 trol (MAM contours, zonally averaged). Fields are the multi-model mean of the models that
741 followed the full TRACMIP protocol in setting up land points. (b) Vertical velocity omega
742 profiles during SH summer (as in a) but averaged over the latitude of tropical ascent and
743 plotted for each individual model (solid for LandControl and dashed for AquaControl; note
744 that we plot negative values both right and left of the vertical zero line, to allow for a cleaner
745 comparison of the profile shape in LandControl (left) and AquaControl (right). (c) and (d):
746 As in (a) and (b), but for the average of the two MetUM models, which did not reduce land's
747 heat capacity. Southern Hemisphere summer season is therefore defined as MAM for both
748 LandControl and AquaControl. 48

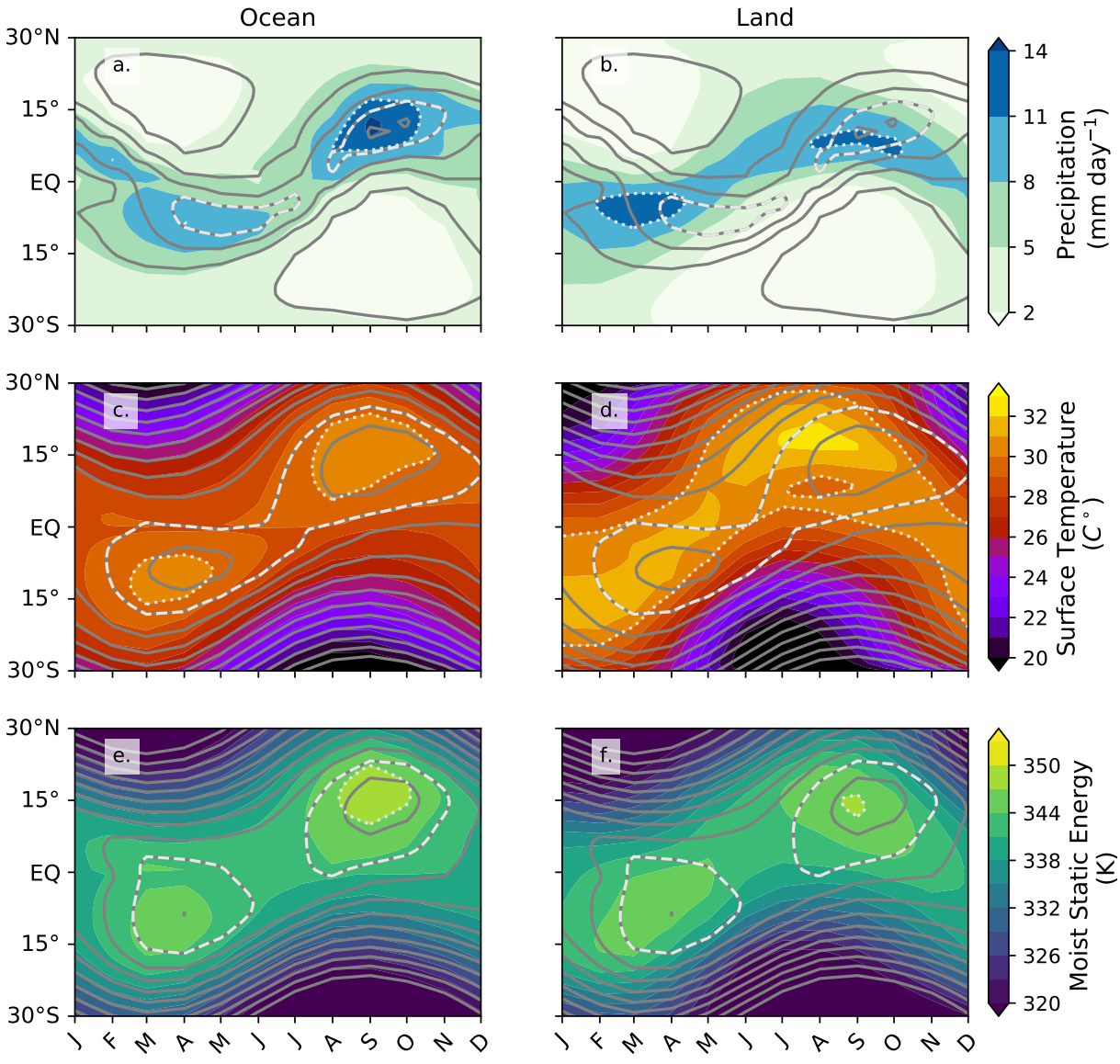

749 FIG. 1. Latitude-Month Hoevmoeller diagram of the climatological ocean (left: a,c,e) and continent (right:
750 b,d,f) sector mean of the LandControl precipitation (a,b), surface temperature (c,d), low-level MSE (e,f). The
751 AquaControl fields are repeated as contours superimposed on the LandControl shading for reference. In all
752 panels, the same contour level is dashed in the AquaControl and dotted in the LandControl to facilitate the
753 comparison of the timing and intensity of the maxima in each field (refer to the colorbar to identify the values
754 corresponding to the highlighted contours).

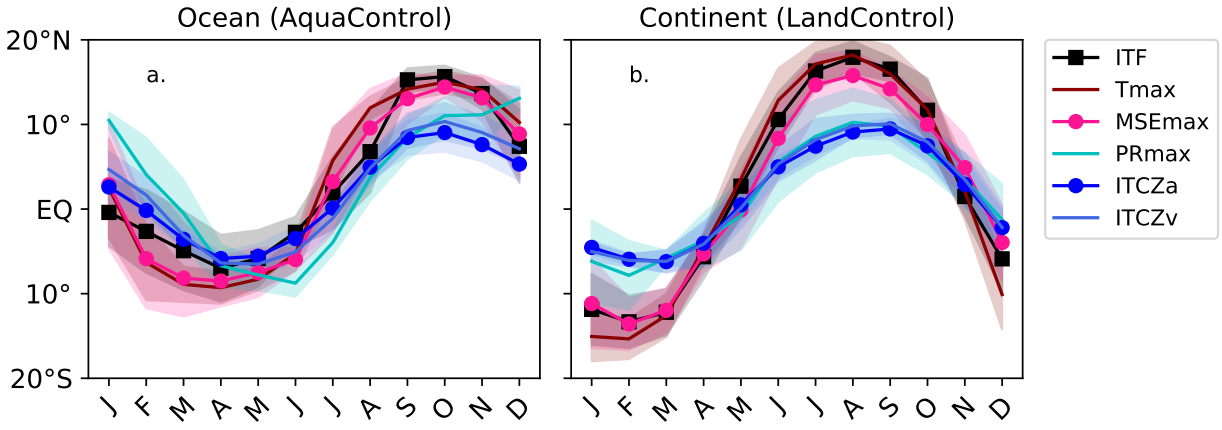

FIG. 2. Meridional positions, as a function of climatological month, of the ITCZ (ITCZa and ITCZv indicate the definitions of Adam et al (2016) and Voigt et al (2014), respectively; blue lines), the maximum in rainfall (light blue), the minimum in SLP (indicated as the InterTropical Front, ITF, black), the maximum in surface MSE (magenta), and the maximum in surface temperature (red). Left panel (a) is for the ensemble and zonal mean of the AquaControl simulations, right panel (b) is for the ensemble and continent sector mean of the LandControl simulations. Shading indicates one standard deviation in the multi-model ensemble.

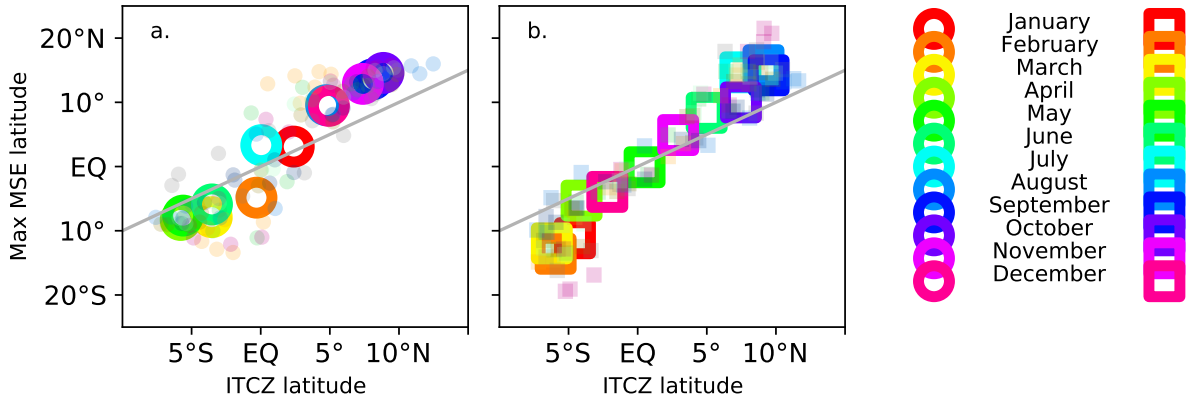

761 FIG. 3. Scatter plots of the (a) zonal-mean AquaControl and (b) sector-mean LandControl latitude of the
762 maximum low-level MSE as a function of the latitude of the ITCZ. Small symbols are for the climatologies of
763 individual models, large symbols are for the multi-model means.

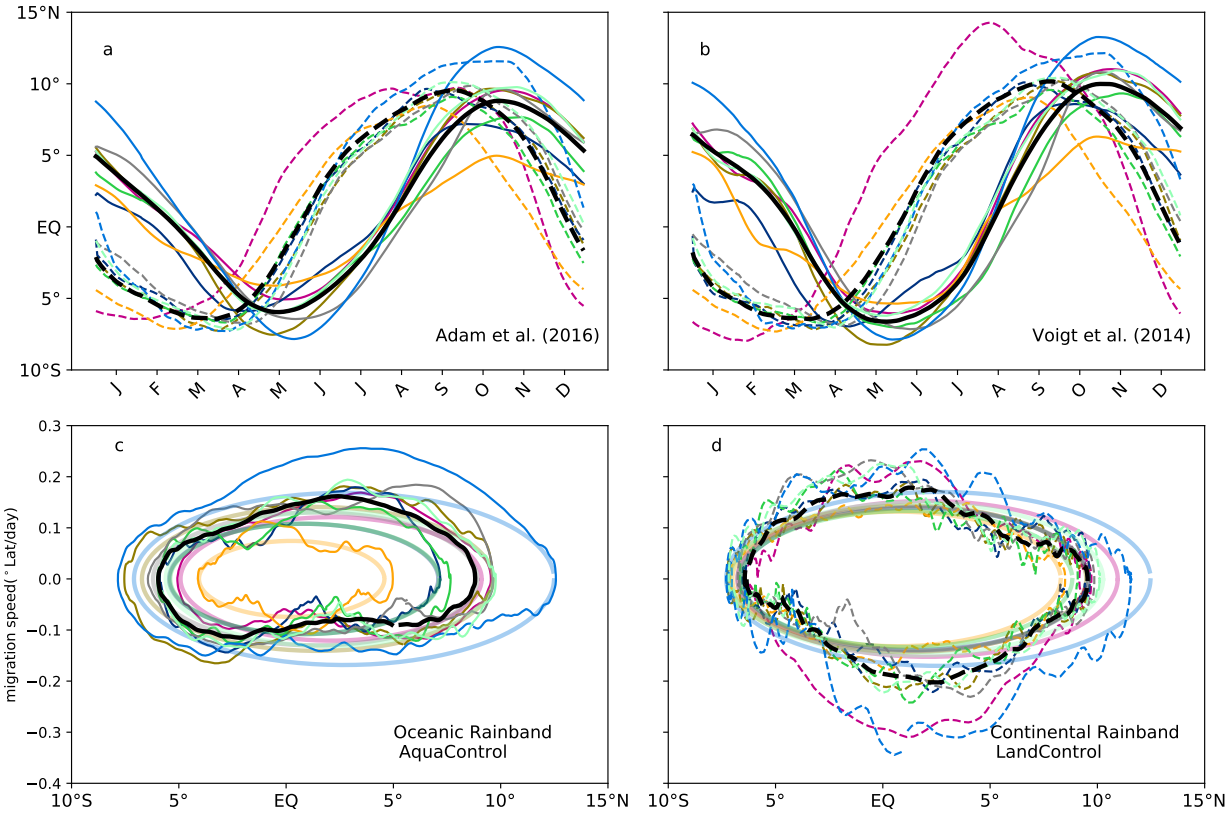

764 FIG. 4. Top (a,b): Position of the ITCZ in the AquaControl (solid lines) and LandControl (dashed lines)
765 according to the definition of Adam et al (2016, a) and Voigt et al (2014, b) as calculated from smoothed
766 daily data. Bottom (c,d): the speed of meridional migration of the ITCZ (according to the Adam et al. (2016)
767 definition) in the AquaControl (c, solid lines) and in the LandControl (d, dashed lines). The perfect ellipses in
768 c and d are obtained by fitting the ITCZ position with two Fourier components (time mean plus a single annual
769 sinusoid) and plotting the corresponding position and velocity. Migration speeds outside the ellipses correspond
770 to rapid transitions. Individual models are color-coded (see Figure 4 for a legend), the multi-model mean is
771 given by the thick black lines.

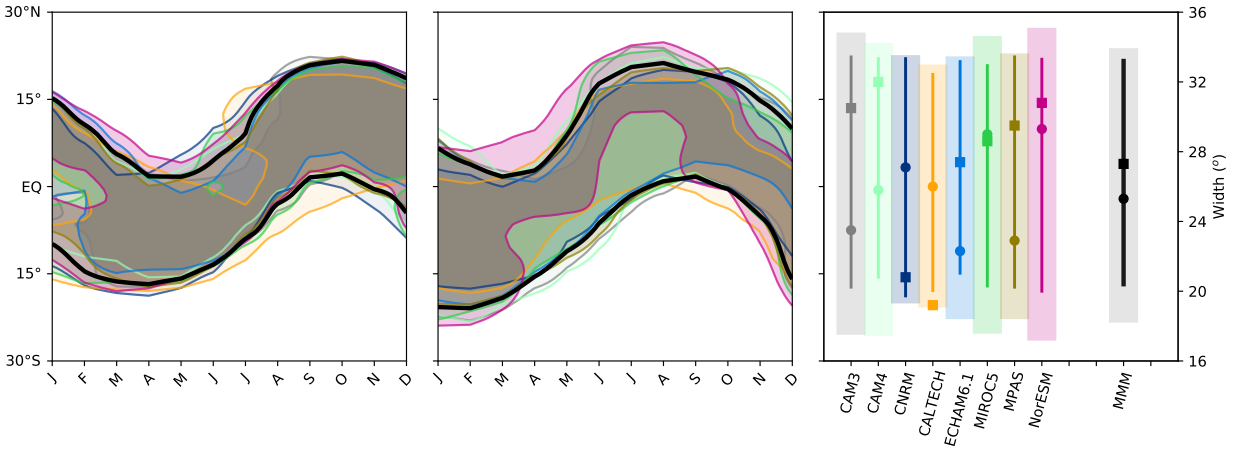

FIG. 5. Width of the ITCZ as indicated by the zero contour of the P-E field. The left panel is for the zonal mean of the AquaControl simulations; the middle panel is for the sector mean of the LandControl simulations. The right panel indicates the meridional span of the ITCZ in its seasonal march (the southernmost reach of the southern zero P-E contour and the northernmost reach of the northern zero P-E contour); broad bars for the LandControl case and thin lines for the AquaControl case; y-axis on the left, corresponding to that on the other panels. The right y-axis measures the maximum width of the ITCZ (distance between the southern and northern zero P-E contours) during the course of the year for the AquaControl zonal mean rain band (dots) and the LandControl sector mean continental rain band (squares). Individual models are color-coded as indicated in the right panel, the multi-model mean is given by the thick black lines.

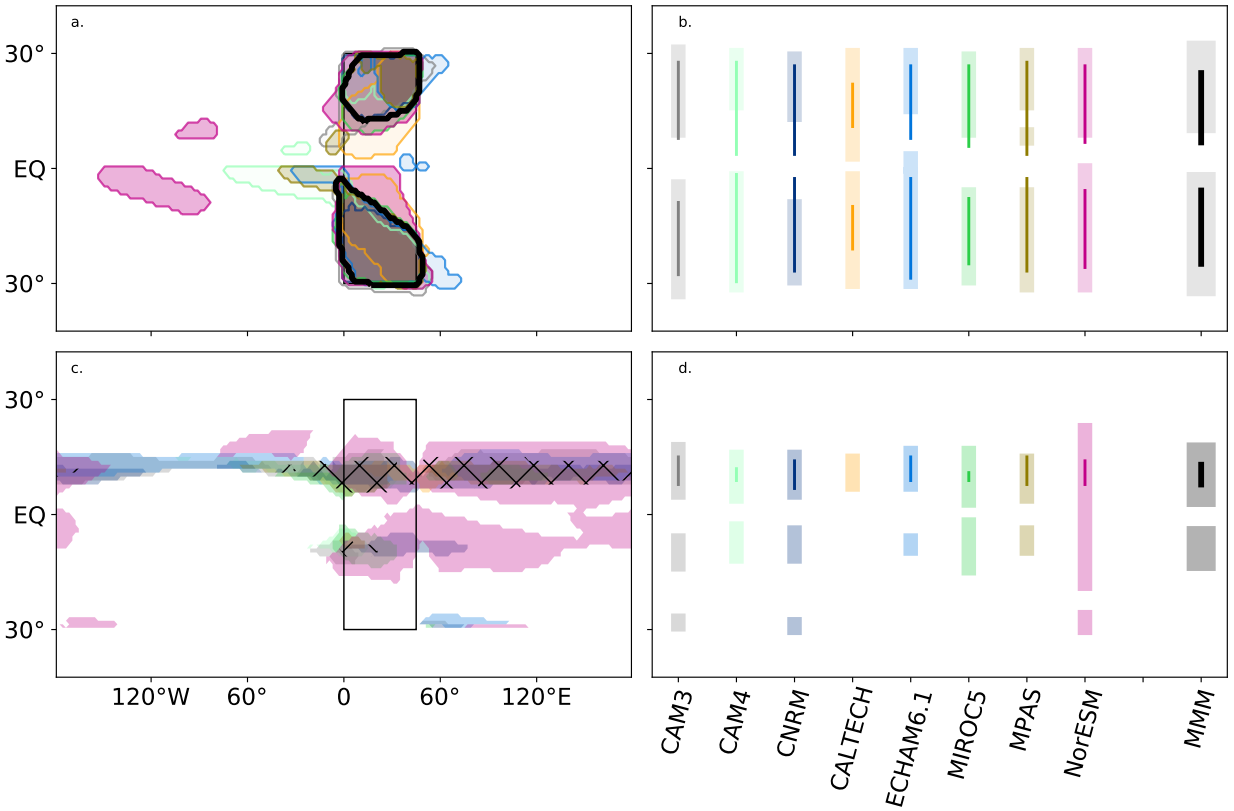

FIG. 6. Spatial extent of the summer rain bands (top) and loci of seasonal wind reversal (bottom). a: Map of the LandControl global monsoon, as defined by a precipitation criterion. Each model is color-coded as indicated in the right-hand panel and the multi-model mean is indicated in black. b: maximum meridional summer extent of the rain-defined global monsoon domain in each model (bars are for the LandControl case and thin lines are for the AquaControl case) and in the multi-model mean. c. Map of the LandControl global monsoon, as defined by a wind reversal criterion. Each model is color-coded and the multi-model mean is hatched in black. d: as in b, but for the wind-reversal criterion. Refer to the text for the exact definition of the rainfall and wind criteria for the global monsoon in the Land and Aqua cases.

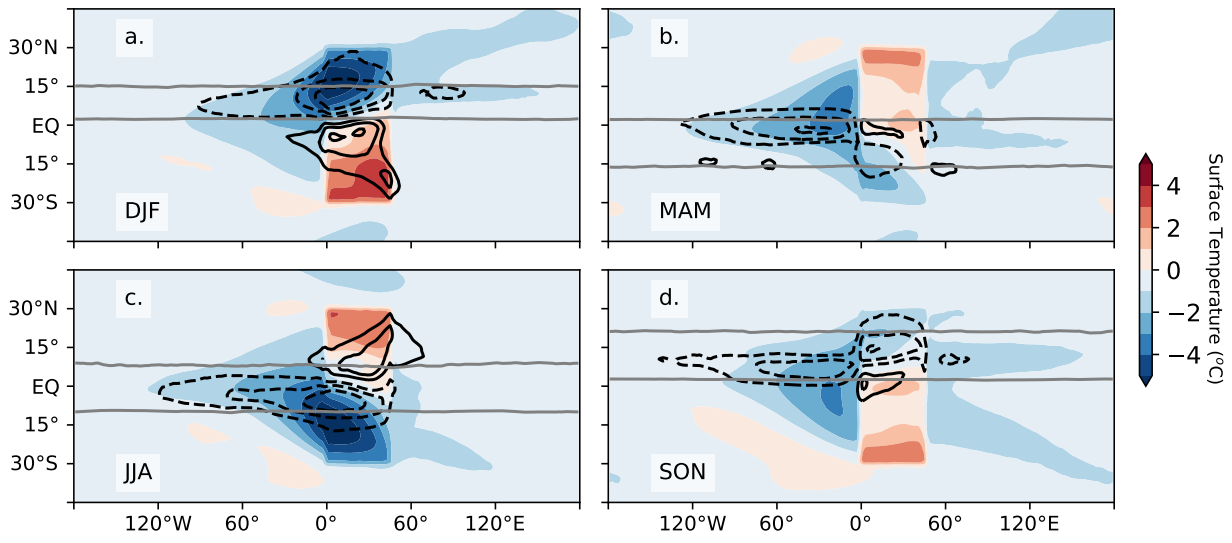

FIG. 7. Maps of the surface temperature (shaded) and precipitation (black contours, every 2mm day^{-1}, skipping the zero contour) LandControl minus AquaControl ensemble-mean seasonal anomalies. The seasonal means are DJF (a), MAM (b), JJA (c) and SON (d). The position of the AquaControl rain band for each season (as indicated by the 6mm day^{-1} contour) is superimposed in grey for reference.

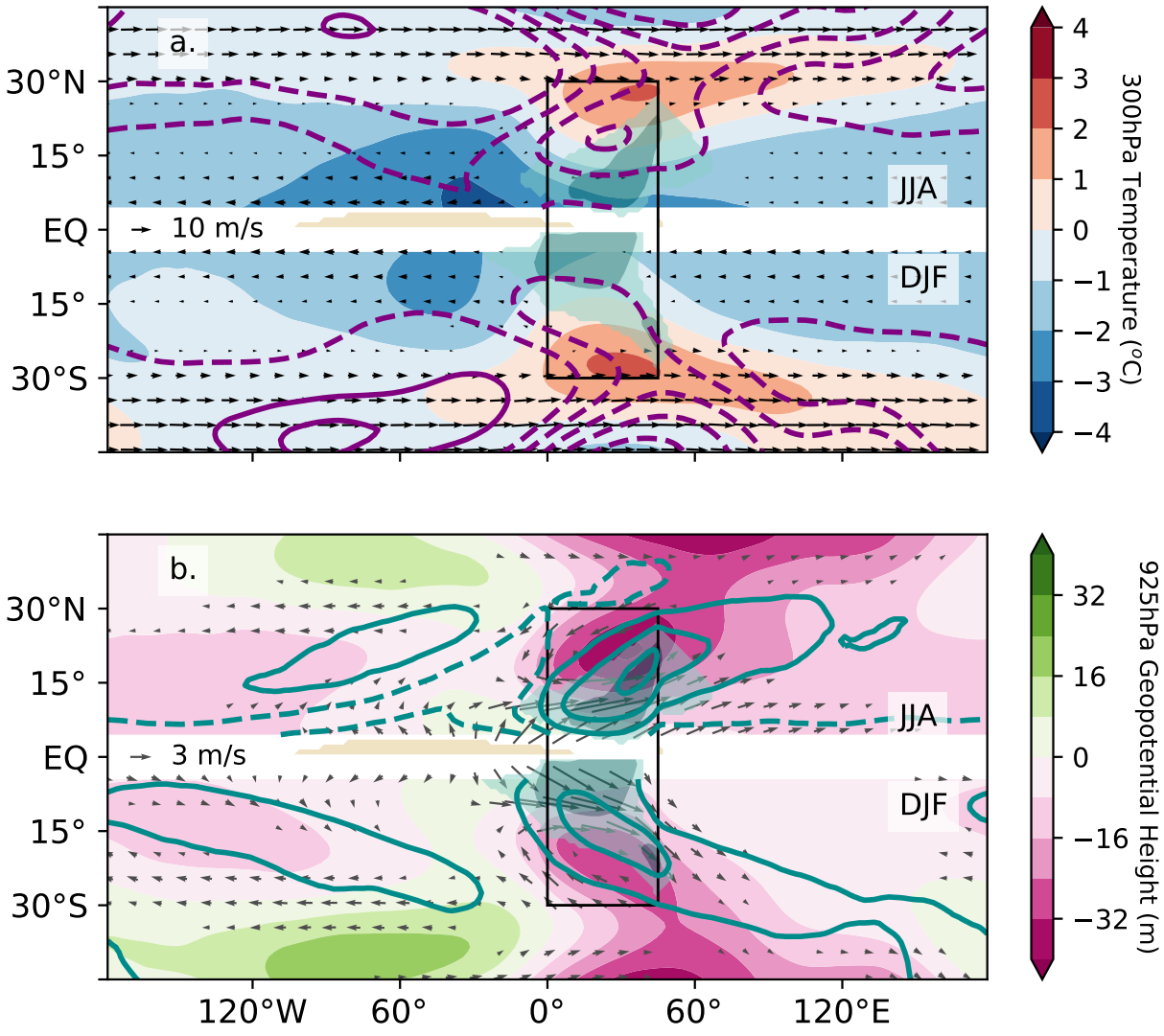

FIG. 8. Top (a): summertime (JJA in the NH and DJF in the SH) ensemble mean LandControl minus AquaControl ensemble-mean anomalies in 300hPa temperature (shaded) and in 700hPa geopotential (contours, contour interval is 8m; dashed lines indicate negative anomalies, the zero contour is omitted), and 700hPa LandControl full wind field (vectors; only wind speeds greater than 3m/s are plotted; see reference arrow on the left). Summertime rainfall anomalies less than -2mm day^{-1} are shaded in brown and those greater than 2 (4) are shaded in green (dark green); Bottom (b): Same as in (a), but shading indicates 925hPa geopotential heights; contours indicate precipitable water (contour interval is 5g Kg^{-1}); and wind vectors are for the 925hPa anomalies (only wind speeds larger than 1m/s are plotted, see reference arrow on the left).

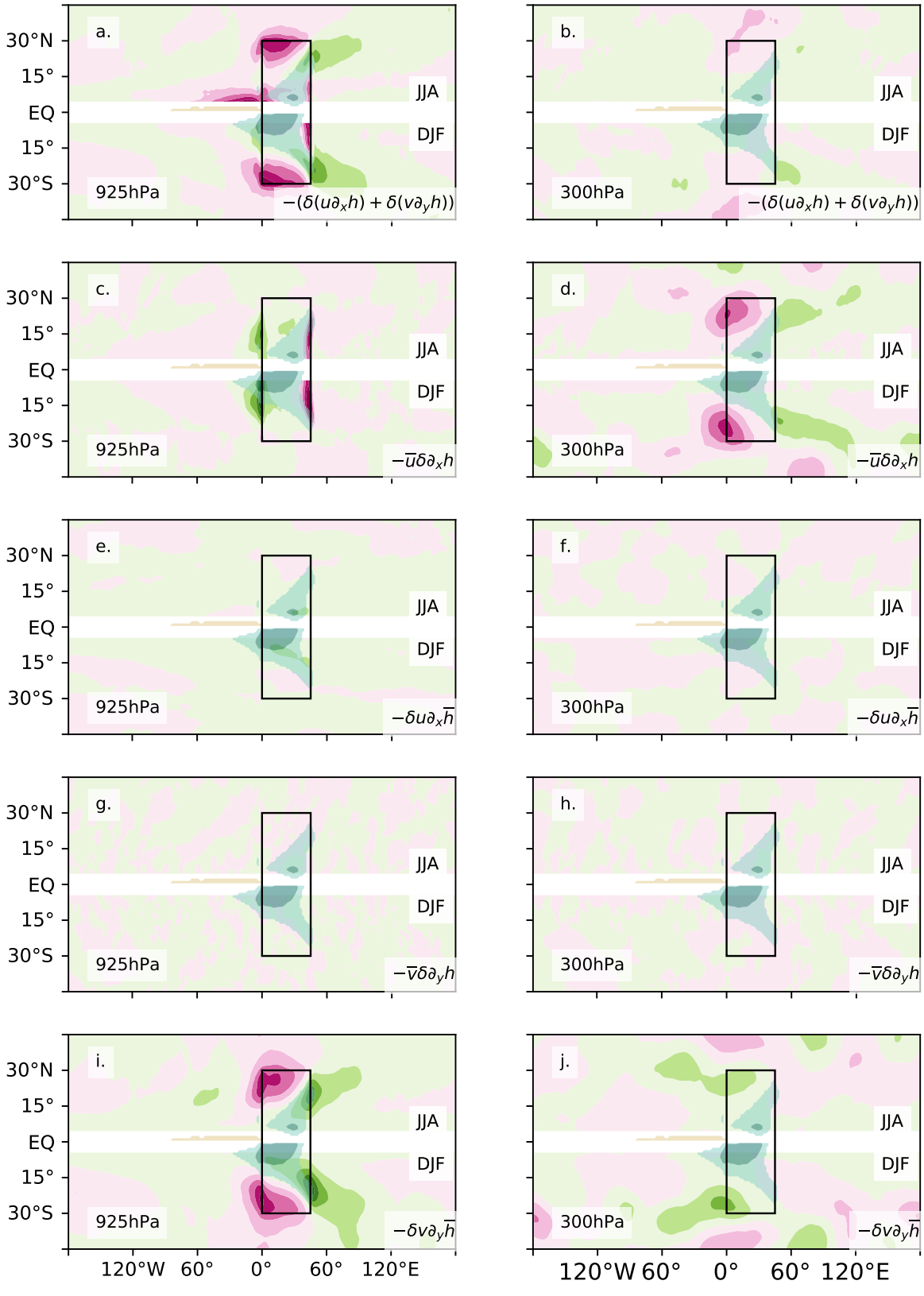
a.
b.
c.
d.
e.
f.
g.
h.
i.
j.
30°N
15°
EQ
15°
30°S
JJA
DJF
925hPa
300hPa
$-(\delta(u\partial_x h)+\delta(v\partial_y h))$
$-\overline{u}\delta\partial_x h$
$-\delta u\partial_x \overline{h}$
$-\overline{v}\delta\partial_y h$
$-\delta v\partial_y \overline{h}$
120°W
60°
0°
60°
120°E
−2.0
−1.5
−1.0
−0.5
0.0
0.5
1.0
1.5
2.0
MSE advection

FIG. 9. Maps of summertime (JJA in the NH and DJF in the SH) LandControl minus AquaControl ensemble-mean anomalous MSE transport at 925hPa (left: a,c,e,g,i) and 300hPa (right: b,d,f,h,l). The total advection anomalies are given in the top panels (a,b). The other panels show: (c,d) the advection of the anomalous MSE gradient by the basic-state zonal wind; (e,f) the advection of the basic-state MSE gradient by the anomalous zonal wind; (g,h) the advection of the anomalous MSE gradient by the basic-state meridional wind; and (i,l) the advection of the basic-state MSE gradient by the anomalous meridional wind. Units are in $^{\circ}$C m s^{-1} (lat/lon degree)$^{-1}$.

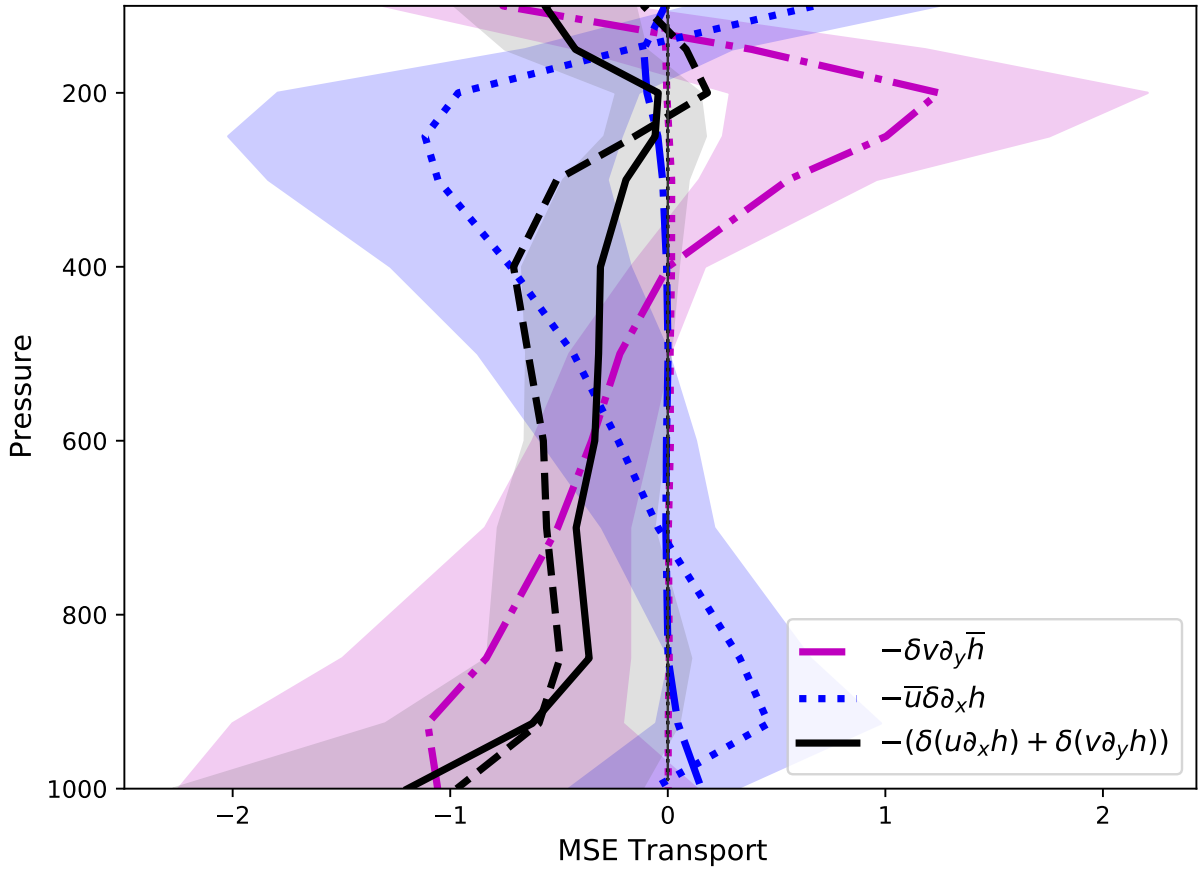

FIG. 10. Vertical average profile of summertime (JJA in the NH and DJF in the SH) LandControl minus AquaControl ensemble-mean anomalous MSE transport in the western subtropical corners of the TRACMIP continent. The total advection anomalies are given in black (the sum of the linearized terms is given in the dashed black line). Blu refers to the advection by the mean wind of the anomalous MSE, magenta refers the advection by the anomalous wind of the mean MSE. Dotted lines refer to zonal terms and dash-dotted lines to meridional terms. The dominant terms are indicated in the legend and are plotted with a shading corresponding to plus or minus one standard deviation in the multi-model ensemble. The vertical axis is pressure in hPa; the MSE transport terms are calculated in units of $^{\circ}$C m s^{-1} (lat/lon degree)$^{-1}$.

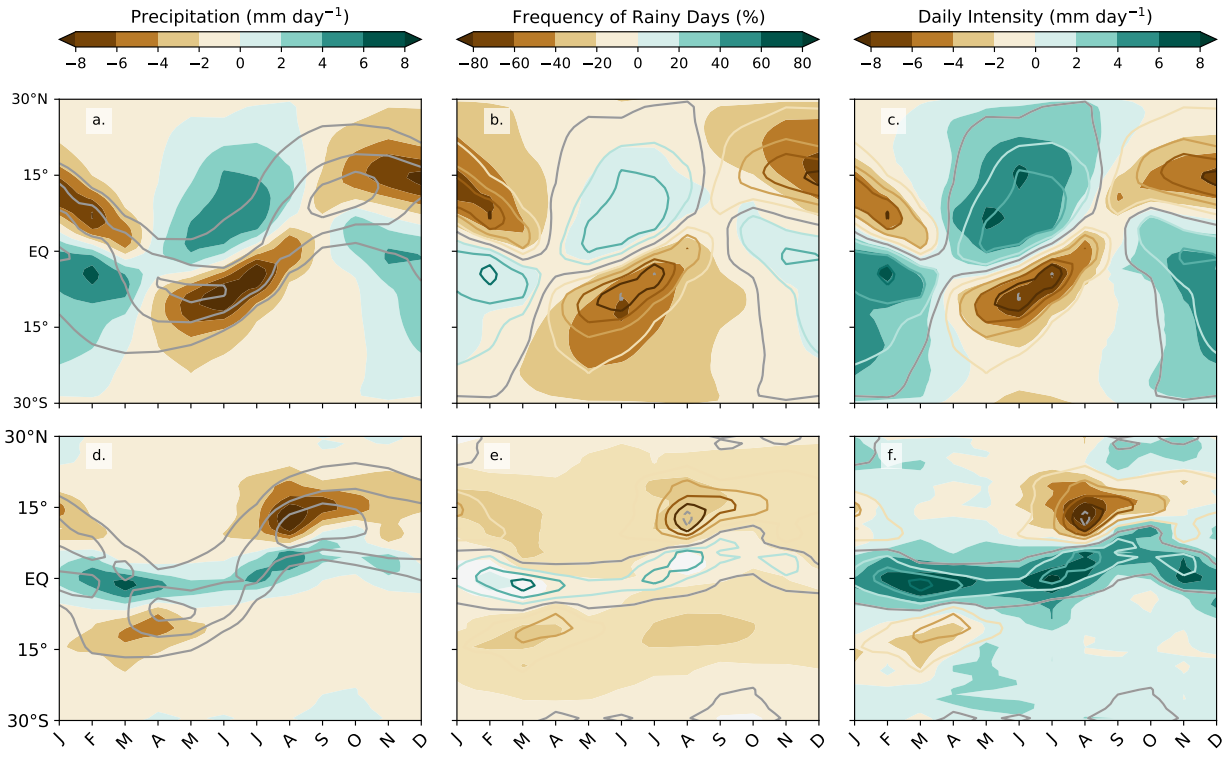

816 FIG. 11. Latitude/time Hoevmoeller diagram of climatological LandControl minus AquaControl multi-model-
817 mean monthly anomalies in (a,d) rainfall in mm day^{-1} (b,d) frequency of rainy days in percentage, and (c,f)
818 simple daily intensity index in mm day^{-1}. Superimposed on the shaded fields are (a,d) the AquaControl climato-
819 logical rainfall (gray contours) and (b,c,e,f) the LandControl-AquaControl monthly rainfall anomalies (contours
820 colored according to the colorbar in a). Top (a,b,c) is for the mean of the models with reduced heat capacity over
821 land. Bottom (d,e,f) is for the average of the models with unchanged heat capacity.

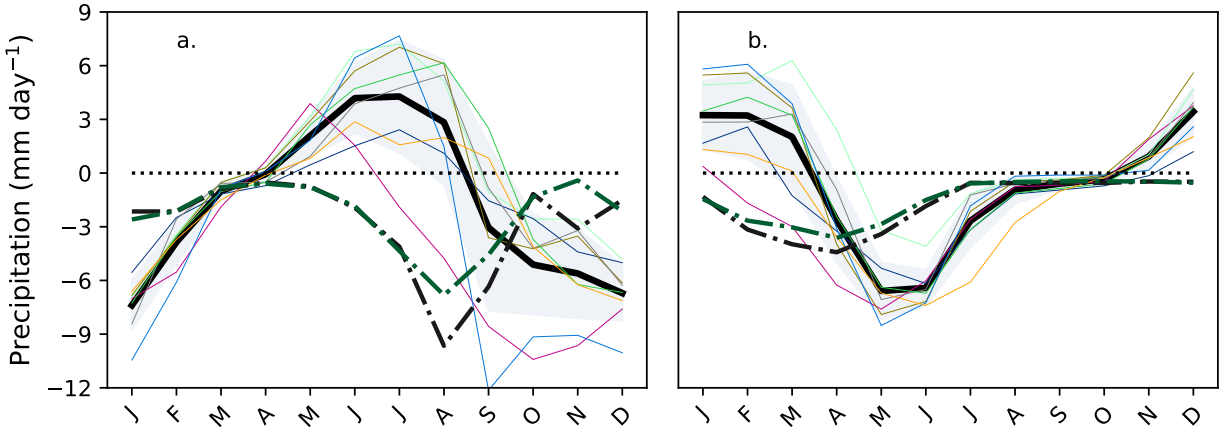

822 FIG. 12. The annual cycle of LandControl minus AquaControl rainfall anomalies averaged zonally (Land-
823 Control data over the continental sector only) and over (a) 10°15° N and (b) 10°15° S . The solid thin colored
824 lines are individual models that followed protocol, the thick solid black line is their multi-model mean, and the
825 light shading indicates a spread of ± 1 standard deviation. The dash-dotted lines are the two models that did not
826 reduce heat capacity in the continental area.

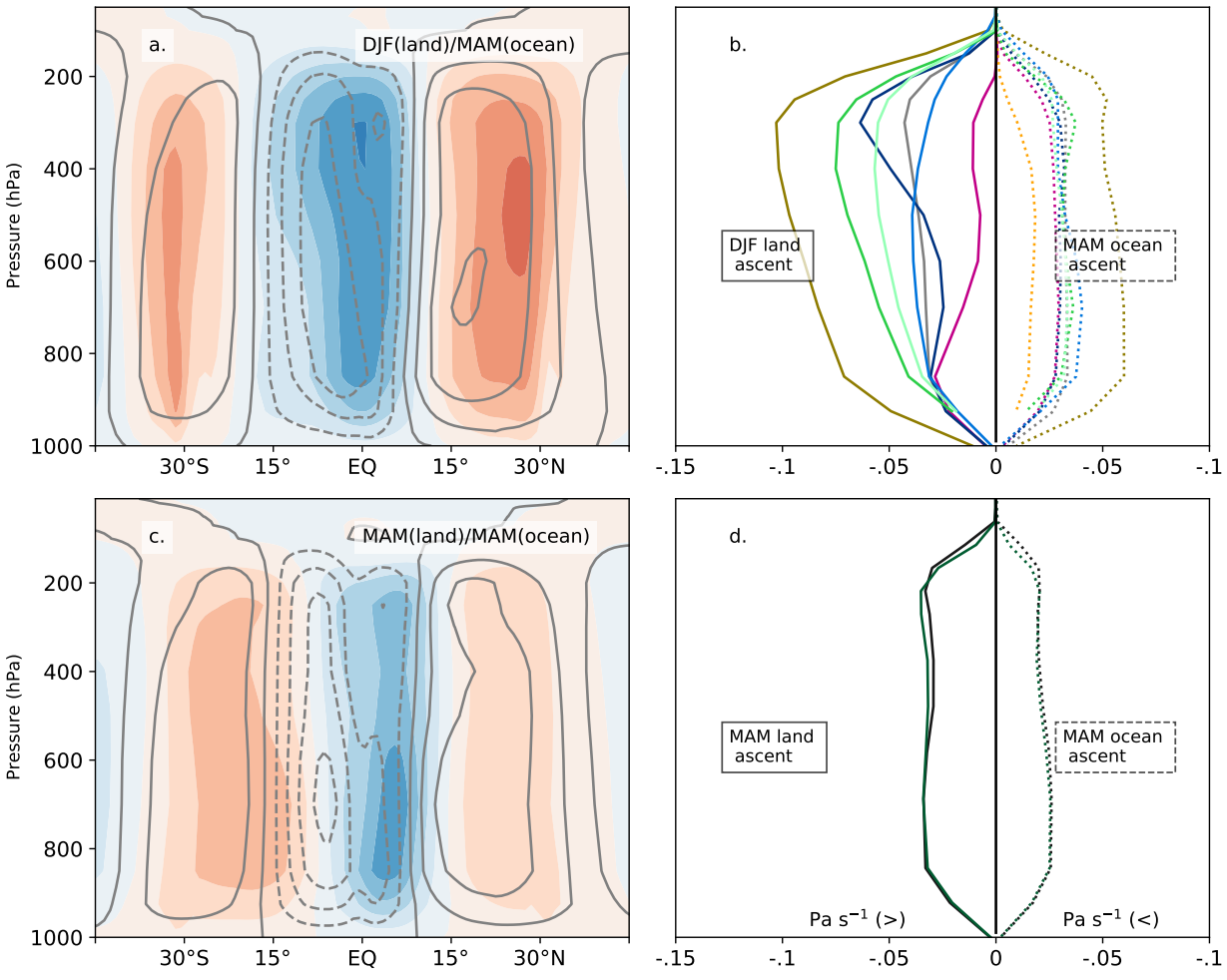

827 FIG. 13. The effect of heat capacity on ascent profiles. (a) Vertical velocity omega profiles during SH summer
828 in LandControl (DJF, shaded, averaged over the continental sector) and AquaControl (MAM contours, zonally
829 averaged). Fields are the multi-model mean of the models that followed the full TRACMIP protocol in setting
830 up land points. (b) Vertical velocity omega profiles during SH summer (as in a) but averaged over the latitude of
831 tropical ascent and plotted for each individual model (solid for LandControl and dashed for AquaControl; note
832 that we plot negative values both right and left of the vertical zero line, to allow for a cleaner comparison of the
833 profile shape in LandControl (left) and AquaControl (right). (c) and (d): As in (a) and (b), but for the average
834 of the two MetUM models, which did not reduce land's heat capacity. Southern Hemisphere summer season is
835 therefore defined as MAM for both LandControl and AquaControl.